ELSEVIER

Journal of Fluids and Structures 18 (2003) 695–713

JOURNAL OF FLUIDS AND STRUCTURES

www.elsevier.nl/locate/jnlabr/yjfls

Aeroacoustical coupling in a ducted shallow cavity and fluid/structure effects on a steam line

P. Lafon, S. Caillaud*, J.P. Devos, C. Lambert

EDF R&D, Department of Analysis in Mechanics and Acoustics, 1 avenue du Général de Gaulle, F-92141 Clamart, France

Received 15 January 2003; accepted 15 August 2003

Abstract

A pure tone phenomenon has been observed at 460 Hz in a piping steam line. The acoustical energy has been identified to be generated in an open gate valve and to be of cavity noise type. This energy is then transmitted to the main pipe by fluid/structure coupling. The objectives here are to display the mechanism of the flow acoustic coupling in the cavity and in the duct through an aeroacoustical analysis and to understand the way of energy transfer from the fluid to the main pipe through a vibroacoustical analysis. Concerning the first objective, an experimental study by means of 2/7 scale models in air is analysed by means of numerical flow simulation. The flow acoustic phenomena are modelled by computing the Euler equations. Two different computations are carried out: in the first one, a pure Euler modelling is used, in the second one, a boundary layer obtained from experimental data is introduced in the computation in order to have a realistic flow profile upstream the cavity. The boundary layer flow profile appears to be essential to recover the experimentally observed coupling between the shear-layer instability and the acoustical transverse mode of the pipe. The numerical results confirm that the second aerodynamic mode is responsible for the oscillation. While the predicted frequency agrees about 1% with the scale model experiments, the predicted amplitude is approximately 15 dB too low. For the second objective, fluid/structure coupling in the main pipe is studied using two fully coupled methods. The first method consists in a modal analysis of the line using a fluid–structure finite element model. The second one is based on the analysis of dispersion diagrams derived from the local equations of cylindrical shells filled with fluid. The way of energy transfer in transverse acoustical waves coupled with flexion-ovalization deformations of the pipe is highlighted using both methods. The dispersion diagrams allow a fast and accurate analysis. The modal analysis using a finite-element model may complete the first one with quantitative data. The link between the fluid/acoustic and the fluid/structure analysis is then the excitation of the transverse acoustical mode of the duct.

1. Introduction

A pure tone acoustical phenomenon has been observed on nuclear power stations. Due to the value of its frequency (460 Hz), the cavity of an open gate valve in the power steam line was immediately suspected. On-site measurements confirmed the source to be located in the gate valve. This aeroacoustical effect is similar to the problem studied by Smith and Luloff (1999). The acoustical energy generated in a shallow cavity is transmitted to the steam lines by fluid–structure coupling. The acoustical transmission to the service building through pipe supports is then a source of disturbance for the nearby workers as reported by Smith and Luloff (1999).

The final objective of the analysis is to find a solution to suppress or reduce the aeroacoustical source in the gate valve. This global analysis is based on experimental measurements and numerical calculations on 2-D and 3-D

*Corresponding author. Tel.: +33-1-47-65-51-18; fax: +33-1-47-65-36-92.
E-mail address: sebastien.caillaud@edf.fr (S. Caillaud).

0889-9746/$ - see front matter
doi:10.1016/j.jfluidstructs.2003.08.018

Nomenclature

c	sound celerity (m/s)
e	specific total energy (J/kg)
d	cavity length (m)
L	cavity inner length (m)
f	frequency (Hz)
h	cavity depth (m)
H	duct height (m)
M	nominal Mach number
p	pressure (Pa)
r	radius (m)
R	radius of the pipe (m)
St	Strouhal number
t	thickness (m)
U_0	nominal velocity (m/s)
x, y	cartesian coordinates (m)
γ	ratio of specific heat
θ	polar angle (rad)
κ	nondimensional wave number
λ	wavelength (m)
ξ, η	curvilinear coordinates (m)
ρ	density (kg/m^3)
σ	scale model
ω	circular frequency (rad/s)
W	nondimensional frequency

Subscripts

c	convection
f	fluid
n	circumferential order
m	longitudinal order
ac	actual
mo	model
T	transpose matrix
x	x derivative
y	y derivative
0	nominal
Ω	volume of fluid
$\sum$	fluid–structure interface

configurations of the valve. The 2-D analysis is devoted to the identification and the understanding of the phenomena and corresponds to the first objective of the paper. The research of solutions and their validation on 3-D configurations, which are close to that of the valve, will be achieved in a second step. Finally, the objectives here are:

(i) to display the mechanisms of fluid/acoustic excitation in the valve on 2-D configurations,
(ii) to understand the way of energy transfer from the fluid to the main pipe.

Concerning the analysis of the fluid/acoustic excitation, this paper emphasizes experimental and numerical results. First, the problem of the cavity noise is presented for the classical configuration and also for the present configuration. Experimental results to be compared to numerical ones are given. Then, the computational methods used in this work are detailed; Euler equations and numerical schemes are displayed. Finally, computational results are presented and analysed for the present configuration of the cavity.

Concerning the second objective of the paper, experimental tests have been realized on the line, which shows that the main steam line exhibits combined flexion-ovalization vibrations but no data are available about the pressure field

inside the pipe. EDF Research and Development has developed a finite-element method (FEM) code of mechanics called Code_Aster (www.code-aster.org), which includes a (u, p, φ) symmetrical formulation for vibroacoustical problems (Morand and Ohayon, 1995; Ohayon and Valid, 1981). Pipes may be for instance modelled using DKT-DST elements of Batoz and Dhatt (1990) and the fluid using (p, φ) 3D-acoustical elements (Morand and Ohayon, 1995). On the other hand, equations of dispersion of pipes filled with fluid are given by De Jong (1994) or Fuller and Fahy (1982) using cylindrical shell theories such as Flügge's (Flügge, 1973) or Donnell's (Fuller and Fahy, 1982; Pavic, 1990, 1992). De Jong (1994) has used dispersion diagrams to justify the use of beam theories and plane waves theory to model piping systems in low frequencies (Seligmann et al., 1998), where shell waves and transverse acoustical waves are evanescent, which is not the case here. These two approaches may be used to explicate the way of fluid–structure energy transfer in the steam line. The acoustical pressure field is unknown even if two scenarios may be possible: there may be plane waves, which are widely studied in low frequencies (Axisa, 2001; De Jong, 1994; Gibert, 1988; Seligmann et al., 1998) or transverse acoustical waves.

The symmetrical FEM and dispersion diagram approaches used here are presented. They are then applied to the steam line. The FEM, which is global, needs to model the whole steam line including the fluid. The dispersion diagram method, which is local, allows an analysis on one pipe section.

2. Aeroacoustical analysis

2.1. The cavity noise problem

2.1.1. The classical case

It is known that flow past an open cavity (Fig. 1) gives rise to self-sustained oscillations. The main features associated to this phenomenon are given by Rossiter (1964) and Rockwell and Naudascher (1978):

(i) an unsteady shear layer develops from the upstream corner of the cavity,
(ii) the vortices convected in the shear layer interact with the downstream corner of the cavity and a pressure disturbance is generated,
(iii) this disturbance acts as a feedback loop on the separation point at the upstream corner where the shear layer develops,
(iv) due to the phase relationship between the downstream generation of the disturbance and its upstream influence, this pressure feedback selectively amplifies the shear layer and preferred modes of oscillations are produced.

These preferred modes of oscillation are given by the semi-empirical formula of Rossiter (1964):

$$\mathrm{St} = \frac{fd}{U_0} = \frac{n - \zeta}{M + U_0/U_c}, \tag{1}$$

where the values for ζ and U_c/U_0 are 0.25 and 0.57, respectively. Formula (1) is in good agreement with experiments for Mach numbers higher than about 0.5 (Rossiter, 1964; Rockwell and Naudascher, 1978). At lower Mach numbers, the oscillations in the cavity tend to remain very weak, and this explains why few published papers are concerned with these.

For a covered cavity with sufficiently high Mach number, experiments reported by Keller and Escudier (1983) show that the wave field strongly depends upon the confined nature of the inflow. Impingement of vortical structures on the trailing edge is no longer the main excitation mechanism. It is rather due to the impingement against solid boundaries of the mean flow entering the cavity. But, at low Mach numbers, Keller and Escudier (1983) pointed out that

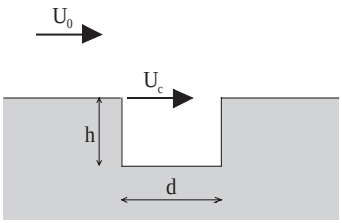

Fig. 1. The classical cavity configuration.

impingement of vortical structures remains the main mechanism for covered cavities too, but with extremely lower RMS values.

Very recently, however, experimental evidence that pronounced flow tones which can be generated at very low Mach number from a fully turbulent inflow past a ducted shallow cavity (Rockwell et al., 2003) has been provided. In this reference, tests have been made with an axisymmetric configuration of the cavity shown in Fig. 1. The authors emphasize conditions giving rise to coherent oscillations, which can lead to locked-on states in the pipe-cavity system. They note that the frequency of the cavity oscillation are correlated with traditional models originally formulated for cavities in free-stream. So, formula (1) should be relevant in that case.

2.1.2. The present case

The geometry retained for the study of the present case is displayed in Fig. 2. The real geometry is quite complex but close to a half-axisymmetric one. The noise source is due to the cavity that houses the disk of the gate valve.

Based upon formula (1), the analysis of on-site measurements shows that in the present case, it is expected that Rossiter's mode 2 is excited. Preliminary 2-D experiments on a wind tunnel in EDF confirm this fact (Devos and Lambert, 2001). Moreover, on-site modal frequencies of the pipe-duct system are very close to the frequency of the cavity noise excitation; so it is also expected that one of them could be excited.

In the present gate valve, down to 0.182 Mach number steam flow, the phenomenon identified is the same as the one described by Rockwell et al. (2003). Rockwell et al. (2003) point out that the behaviour of 2-D and axisymmetric cavities is very similar. So, we should expect the valve cavity well represented by a 2-D modelling. In the classical open cavity noise problem, the nominal velocity U_0 is the free stream velocity; but in the present case, it seems logical to take the maximum velocity in the duct as the nominal velocity.

2.2. Experiments in wind tunnel

Experiments were carried out in a wind tunnel at the Institut AéroTechnique, Saint-Cyr-l'Ecole, and they are well described by Amandolèse et al. (2002). The global scale retained for the experimental model is $\sigma = 2/7$. So, its characteristic dimensions are (Fig. 2): $d = 0.05\,\text{m}$, $h = 0.02\,\text{m}$, $H = 0.137\,\text{m}$, $L = 0.073\,\text{m}$.

The span of the test section has a value of 0.16 m.

For the sake of formula (1), the nondimensional similarity ratios that should be maintained are the Mach number based on the nominal velocity $M_0 = U_0/c$ and the Strouhal number fd/U_0. So, the actual frequencies are related to the model ones by $f_{ac} = \sigma(c_{ac}/c_{mo})f_{mo}$. With these assumptions, the ratio of cavity oscillation frequencies f_{ac}/f_{mo} and the ratio of transverse acoustic mode frequencies in the duct are identical. The sound speed in the wind tunnel is $c_{mo} = 343\,\text{m/s}$, whereas for the thermodynamic state of the steam flow through the valve $c_{ac} = 490\,\text{m/s}$.

The measurements were made using a microphone located at the bottom centre of the cavity (Fig. 2). Experimental spectra are plotted in r.m.s. linear dB, an example is given in Fig. 3, whereas those coming from Euler calculations are expressed in normalized form, so the level does not depend on the filter bandwidth Δf, i.e.:

$$Lp(f) = 10\,\log_{10}\left(\frac{P(f)^2}{\Delta f\ P_0^2}\right), \tag{2}$$

where $P_0 = 2 \times 10^5\,\text{Pa}$ and $P(f)$ is the Fourier transform of the pressure signal. So, due to the experimental bandwidth filter of 0.5 Hz, it is needed to increase experimental plots of 3 dB in order to compare them with numerical ones.

Measurements obtained on the scale model are in agreement with the phenomena observed on-site. Strong oscillations appear at Mach numbers for which mode 2 Rossiter's frequency given by formula (1) is close to the first transverse mode of the duct. Plots of frequency and pressure level as functions of M_0 are shown in Fig. 4. Fig. 5 shows corresponding plots of experimental Strouhal numbers compared to theoretical ones, which are modes 2 and 3 of Rossiter's formula and the first transverse mode of the duct of frequency $c_{mo}/2H$.

The main feature to be noted in Figs. 4 and 5 is that when Rossiter's frequency is close to the duct mode, the frequency of the oscillation locks-on the frequency of the pipe mode. Lock-in phenomena could appear in a wide variety of configurations as shown by Blevins (2001) for instance on the case of vortex shedding from an oscillating cylinder. In the present case, the maximum pressure level of 128 dB is reached at $M_0 = 0.183$ (Fig. 4). Then, the experimental frequency of oscillation is 1216 Hz while Rossiter's formula gives 1206 Hz for mode 2 (with $\zeta = 0.14$) and the calculated frequency of the duct mode is 1263 Hz.

Applying the similarity ratios to the frequency of 1216 Hz measured on the scale model, an actual frequency of 496 Hz that is a little more higher than the frequency of 460 Hz measured on-site is found. That could be linked to the fact that duct mode frequencies are different for the rectangular test section of the model and for the on-site pipe-valve system.

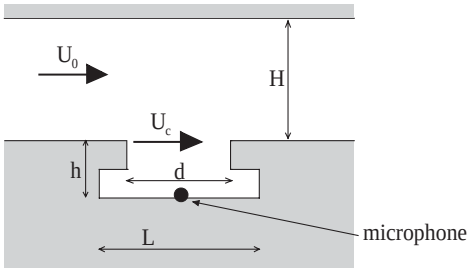

Fig. 2. The cavity studied in this paper.

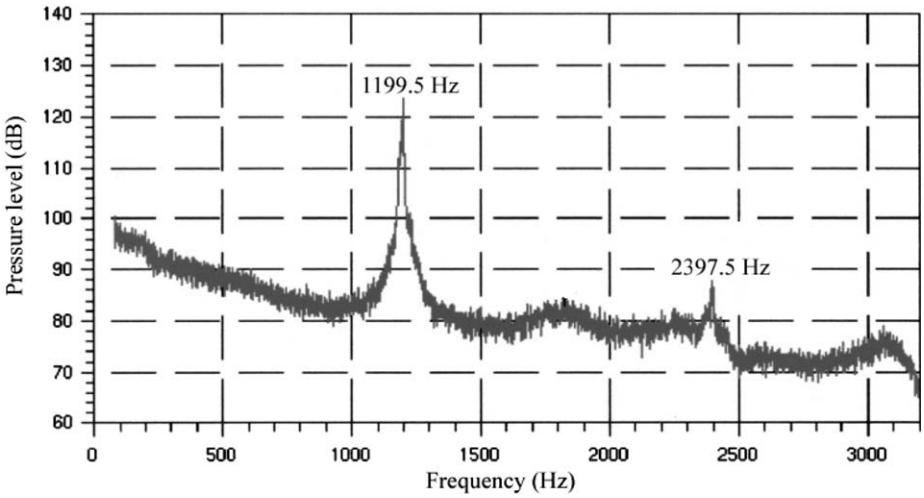

Fig. 3. Pressure spectrum measured inside the cavity model at $M_0 = 0.180$.

As we could already observe on available data in free-stream flow (Rockwell and Naudascher, 1978), Fig. 5 shows that, at low Mach number, Rossiter's formula underestimates the frequency of the cavity oscillation. Assuming that the U_c/U_0 ratio remains constant, in the Mach number range 0.1–0.25 and for the present ratio H/d, a value for ζ of 0.14 fits the experimental data, instead of 0.25. Moving the duct height, a slight increase of the fitted values is displayed for ζ with H, thus with the thickness of the boundary layer ($\zeta = 0.125$ for $H = 0.110$ m; $\zeta = 0.17$ for $H = 0.152$ m).

It must be underlined that the cavity of Fig. 2 is proved to be much more noisy than the classical one of Fig. 1. No oscillation with significant level occurs for experiments carried out with the classical cavity.

2.3. Numerical modelling of the aeroacoustical behaviour of a ducted cavity

2.3.1. The choice of the numerical modelling

Several numerical techniques have been recently used in order to model the aeroacoustical behaviour of cavities. It is possible to use direct numerical simulation (DNS) as in the work of Gloerfelt (2001) and Gloerfelt et al. (2003). It is also possible to use the Euler equations as in the work of Dequand et al. (2003) where self-sustained oscillations in deep cavity are simulated. We made the same choice as Dequand et al. (2003) because upstream boundary layer apart, self-excited cavity oscillations are essentially nonviscous phenomena. So, it is hoped that imposing a description of the upstream boundary layer into an Euler approach would simulate the phenomenon in a satisfactory way. Moreover, this approach offers the advantage to be little costly in CPU time.

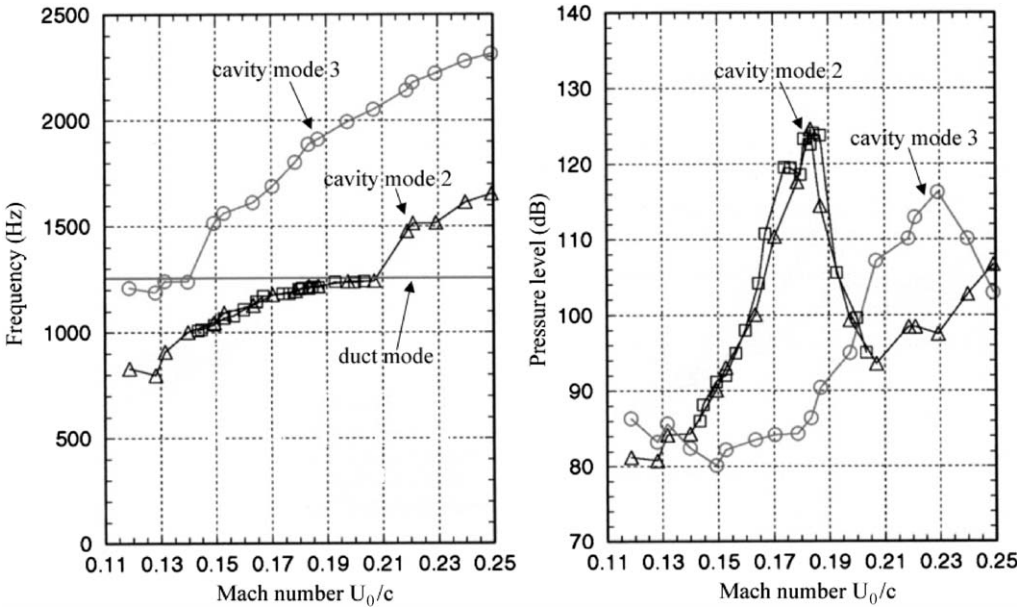

Fig. 4. Frequency and level of pressure oscillations measured inside the cavity model as functions of the Mach number U_0/c.

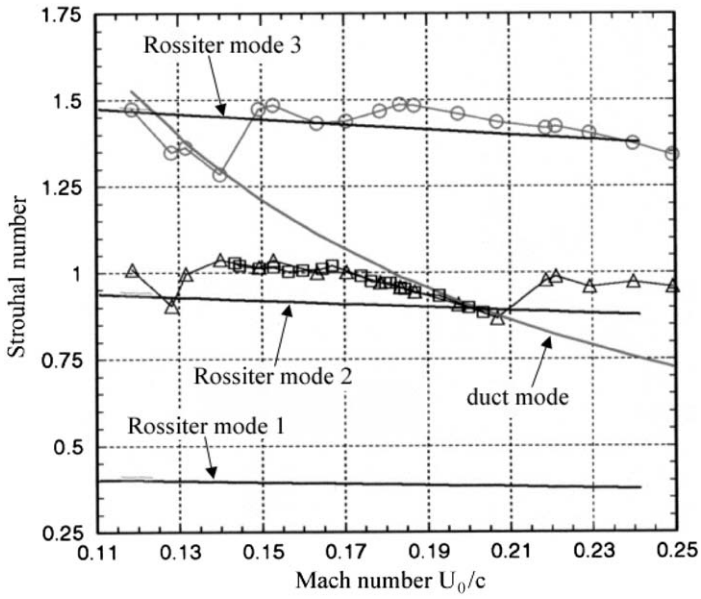

Fig. 5. Strouhal numbers measured inside the cavity model compared to theoretical ones as function of the Mach number U_0/c.

2.3.2. A numerical formulation based on the computation of Euler equations

The present paper emphasizes on calculations carried out with a 2-D curvilinear code based on Euler equations. In two dimensions, the Euler equations are written in strong conservative form as

$$\frac{\partial \vec{W}}{\partial t}+\frac{\partial \vec{F}}{\partial x}+\frac{\partial \vec{G}}{\partial y}=0, \tag{3}$$

where

$$\vec{W} = \begin{bmatrix} \rho \\ \rho u \\ \rho v \\ e \end{bmatrix}, \quad \vec{F} = \begin{bmatrix} \rho u \\ \rho uu + p \\ \rho uv \\ (e+p)u \end{bmatrix}, \quad \vec{G} = \begin{bmatrix} \rho v \\ \rho uv \\ \rho vv + p \\ (e+p)v \end{bmatrix}. \tag{4}$$

The total energy per unit volume is related to the pressure by the equation of state for a perfect gas:

$$p = (\gamma - 1)\left[e - \rho\frac{u^2 + v^2}{2}\right]. \tag{5}$$

In order to be able to compute curvilinear grids, a generalized coordinate transformation is introduced:

$$\xi = \xi(x, y) \quad \text{and} \quad \eta = \eta(x, y). \tag{6}$$

In this new coordinate system, Eq. (3) reads:

$$\frac{\partial \hat{\vec{W}}}{\partial t} + \frac{\partial \hat{\vec{F}}}{\partial \xi} + \frac{\partial \hat{\vec{G}}}{\partial \eta} = 0, \tag{7}$$

where

$$\hat{\vec{W}} = \vec{W}/J, \hat{\vec{F}} = (\xi_x \vec{F} + \xi_y \vec{G})/J, \hat{\vec{G}} = (\eta_x \vec{F} + \eta_y \vec{G})/J. \tag{8}$$

J is the Jacobian of the transformation

$$J = \xi_x \eta_y - \xi_y \eta_x. \tag{9}$$

The equations are discretized using a finite volume upwind formulation (Harten, 1983; Lafon and Devos, 1993; Roe, 1980; Yee et al., 1990):

$$\overrightarrow{\hat{F}}_{i+1/2,j} = \frac{1}{2}\left[\left(\frac{\xi_x}{J}\right)_{i+1/2}\left(\vec{F}_{i,j} + \vec{F}_{i+1,j}\right) + \left(\frac{\xi_y}{J}\right)_{i+1/2}\left(\vec{G}_{i,j} + \vec{G}_{i+1,j}\right) + \rightarrow \vec{R}_{i+1/2,j}\vec{\Phi}_{i+1/2}/J_{i+1/2}\right], \tag{10}$$

where R is the eigenvector matrix. When the second-order upwind scheme is used, the kth element of the vector Φ for the second-order upwind TVD scheme reads:

$$\Phi^k_{i+1/2} = \sigma(a^k_{i+1/2})[g^k_i + g^k_{i+1}] - \Psi\left(a^k_{i+1/2} + v^k_{i+1/2}\right)\alpha^k_{i+1/2}, \tag{11}$$

where

$$\begin{aligned} &\sigma(z) = \frac{1}{2}\Psi(z) \quad \text{and} \quad \Psi(z) = |z|, \\ &g^k_i = \left(\alpha^k_{i+1/2}\alpha^k_{i-1/2} + \left|\alpha^k_{i+1/2}\alpha^k_{i-1/2}\right|\right)/(\alpha^k_{i+1/2} + \alpha^k_{i-1/2}), \\ &\alpha^k_{i+1/2} = \overrightarrow{\vec{R}}^{-1}_{i+1/2} k(\vec{W}_{i+1} - \vec{W}_i), \\ &v^k_{i+1/2} = \sigma(a^k_{i+1/2})\begin{cases} (g^k_{i+1} + g^k_i)/\alpha^k_{i+1/2} & \text{if } \alpha^k_{i+1/2} \neq 0, \\ 0 & \text{if } \alpha^k_{i+1/2} = 0. \end{cases} \end{aligned} \tag{12}$$

In order to ensure second-order time accuracy, a Runge–Kutta algorithm is used for the temporal discretization:

$$\begin{aligned} \vec{W}^* &= \vec{W}^n - \Delta t H(\vec{W}^n), \\ \vec{W}^{n+1} &= \tfrac{1}{2}(\vec{W}^n + \vec{W}^* - \Delta t H(\vec{W}^*)). \end{aligned} \tag{13}$$

The computational domain size is $2\,\text{m} \times 0.17\,\text{m}$. The minimum mesh size near the cavity is $5 \times 10^{-5}\,\text{m}$. The mean time step is $7 \times 10^{-8}\,\text{s}$. The important length of the computational domain upstream and downstream the cavity is obtained by slowly increasing the mesh size in the longitudinal direction. So boundary conditions are treated far from the cavity and acoustic waves propagating from the cavity through the duct are gradually absorbed. Boundaries and initial conditions were implemented in a way similar that Dequand et al. (2003) did it for their own Euler computations.

For the inlet and the outlet boundary conditions, it is expected that acoustic waves are going to be absorbed because of the increasing mesh size. But, in order to minimize the influence of boundary conditions, the classical treatment of boundary conditions, which used characteristic variables and compatibility equations, need to be modified. The usual

configurations that were implemented, subsonic inlet, supersonic inlet, subsonic outlet and supersonic outlet, are completed by two new configurations, nonreflective subsonic inlet and nonreflective subsonic outlet. The difficulty of imposing at the boundaries both flow variables such as pressure and a nonreflective treatment is overcome by introducing in the equations additional terms that drive the solution towards a target state at infinity (Poinsot and Lele, 1992). Here, the additional terms introduced in the right-hand side of the system of Eq. (3) are for the mass equation $(\alpha_0/\mathrm{d}t)(\rho_\infty - \rho)$ and for the momentum equations $(\alpha_0/\mathrm{d}t)(\rho_\infty u_\infty - \rho u)$ and $(\alpha_0/\mathrm{d}t)(\rho_\infty v_\infty - \rho v)$. In the characteristic direction $\mathrm{d}x/\mathrm{d}t = u + c$ for instance, the previous treatment declines as

$$\mathrm{d}p + \rho c\,\mathrm{d}u = \alpha_0[(\mathrm{p}_\infty - p) + \rho_\infty c(u_\infty - u)]. \tag{14}$$

This technique, which allows the waves to travel through the inlet or outlet boundaries, is a "weak" way to impose flow conditions in the upstream boundary layer. The corrective terms on pressure and u component of velocity are, respectively, $\alpha_0(p_\infty - p)$ and $\alpha_0(\rho_\infty/\rho)(u_\infty - u)$, where u_∞ is the average velocity of the boundary layer profile at the calculated point. Numerical tests prove that on the frequency range of analysis, the waves are allowed to travel freely with the parameter α_0 set to 100.

For initial conditions in the duct, outside the cavity, an homogeneous pressure field and a constant velocity profile were imposed. Inside the cavity, the mean pressure was the same as that in the duct and the mean velocity was zero. In order to initiate oscillations, a small initial perturbation has to be imposed. We choose to make it by modifying pressure and velocity fields inside the cavity with the application of a longitudinal harmonic standing wave. The maximum amplitude of the pressure field, at the walls, was 1.0 Pa.

2.3.3. *Application with a nonviscous wall boundary condition*

In this first calculation, because of the assumption made (Euler equations modelling), there is no difference between nominal velocity and mean velocity in the duct (considering the boundary layer thickness is zero). So, we impose at the inlet the maximum velocity $U_0 = 62.8$ m/s measured on the experimental profile in the duct. The spectral analysis of the time evolution of the pressure in the cavity shows that the frequency of the excitation captured in the computation is around 2000 Hz. Two main eddies are present in the shear layer which is typical of the mode 2 of excitation.

The phenomenon is only partially captured by this first computation. The excitation due to the cavity noise is qualitatively retrieved: Rossiter mode 2 is identified. But, the frequency that is exhibited by the calculation (2000 Hz) is much higher than the experimental one (1216 Hz). Moreover, this computed frequency is also by far different from the first transverse acoustic mode so that no coupling is able to occur between the cavity excitation and the duct mode. It seems that the convection velocity of the eddies in the shear layer is far from the classical value of $0.57U_0$: in this first calculation, this value appears to be very close to U_0 because the estimated frequency of Rossiter's mode 2 with is 1840 Hz. So the shear layer seems to behave as if the eddies were convected with . This may be due to the absence of physical viscosity in the fluid modelling. This absence is perhaps less crucial in the shear layer than in the wall boundary layer upstream cavity corner where the shear layer development starts.

At the upstream trailing edge, the situation is indeed very different if the velocity profile is uniform as in Fig. 6(a) or follows a classical wall law as in Fig. 6(b). One could think the convection velocity of the eddies depends on the velocity of the mean flow at the streamlines that drive the vortex through the cavity. In the present case, all the streamline velocities are closed to U_0. With an actual viscous boundary layer the vortex would be convected along streamlines with much lower mean velocities. This influence of the upstream boundary layer on the cavity noise has been pointed out in previous works especially by Sarohia (1977).

2.3.4. *Application with a viscous wall boundary condition*

In order to overcome the problem due to the absence of a real boundary layer modelling in the Euler computations, a second calculation is carried out in which the wall flow profile determined experimentally is imposed upstream the cavity. As for the boundary conditions at the inlet, we want the waves to travel freely; so, at every time step, between the inlet and the cavity, the experimental wall flow profile is "weakly" imposed as it is done for the inlet boundary condition treatment. The same profile is also imposed as the inlet boundary condition. The following law that fits correctly the

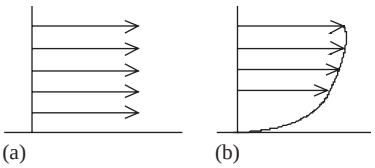

Fig. 6. (a) Uniform velocity profile and (b) classical wall law.

experimental data is used:

$$\frac{u(y)}{U_0} = \left(\frac{y}{\delta}\right)^{1/n} \tag{15}$$

with $\delta = 8.8$ mm and $n = 8.5$. For $y \geqslant \delta$, no correction was imposed. In the logarithmic region of the boundary layer profile, the previous law is close to the following one for a smooth pipe:

$$\frac{u(y)}{U_f} = 5.75 \log_{10}\left(\frac{y\rho U_f}{\mu}\right) + 5.24, \tag{16}$$

where with $U_0 = 62.8$ m/s, the friction velocity U_f is 2.65 m/s.

2.4. Analysis and discussion

The temporal evolution of the pressure derived from a numerical sensor on the top wall of the duct in front of the cavity is given in Fig. 7. Pressure signal at the top wall is more eloquent because only acoustic component is present. A spectral analysis of the pressure signal shows that the oscillation retrieved by the calculation is around 1200 Hz. This computational value lies very close to the experimental one (1216 Hz).

Fig. 8 displays a comparison of calculated and measured spectra inside the cavity. In the calculated spectrum, the oscillation level is 108 dB (there is a mistake in the original paper by Lafon et al. (2002), where "129 dB" is indicated) whereas the measured one is 125 dB. Spectra were calculated after removing the transient part, which is the duration needed to get an established flow inside the cavity. In the model conditions (Fig. 7), a transient part of 0.025 s was taken into account.

All previous results came from calculations carried out for $M_0 = 0.183$, which is the Mach number of higher experimental pressure amplitudes. In order to evaluate the ability of the numerical scheme to retrieve the variation of the phenomenon amplitude with the Mach number, two other calculations were carried out for $M_0 = 0.15$ and 0.21. The oscillation spectra given by the three calculations are superimposed in Fig. 9. The experimental evolution of oscillation levels with respect to the Mach number is qualitatively retrieved by the computations. For $M_0 = 0.15$ to 0.21, amplitude of mode 3 should be increasing as observed on experimental results of Fig. 4. However, such peak for mode 3 is not retrieved by the computations.

The results obtained by the second calculation carried out with the addition of a viscous wall boundary condition upstream the cavity show clearly that the influence of this modelling point is essential to obtain a satisfactory simulation. It is seen in Fig. 4 that the oscillation amplitude is not constant in time. Fig. 10 shows five successive pictures of the pressure and vorticity fields in the duct during the period of an high amplitude oscillation. The two main eddies in the shear layer, which are typical of the Rossiter's mode 2, are present. Examining fields of vorticity, it seems that amplitude depends on the size of the vortex and whether they hit the downstream edge of the cavity or not. Fig. 11 shows a field of vorticity during a period of low oscillation. One can see that a vortex has just over passed the downstream edge.

Finally, it appears clearly that the acoustic source due to the cavity radiates in phase with the first transverse mode of the duct: this indicates that the two modes are coupled. However, computation underestimates the pressure level for more than 15 dB. In other applications involving Euler computations, we were used to get overestimates. However, Dequand et al. (2003) also notes an underestimation of amplitude by their Euler calculations for a deep cavity. Spectra in Fig. 8 show that broadband fluctuations inside the cavity are, on the contrary, overestimated by calculations. That could be due to the lack of viscous effects in the model. Then, the higher level of broadband fluctuations would abnormally disturb coherent fluctuations in the cavity and so that would lead to underestimation of the oscillation level.

3. Vibroacoustical analysis

3.1. Numerical formulations

3.1.1. FEM formulation (u, p, φ)

The fluid–structure formulation used here with Code_Aster is derived from Morand and Ohayon (1995) and has already been used in FEM codes, for instance, by Axisa (2001) and Gibert (1988). The introduction of a potential of fluid displacement φ by Ohayon and Valid (1981), $\vec{u}_f = \overrightarrow{\text{grad}}\,\varphi$, gives a symmetric formulation of the problem, which has been introduced in the FEM code Code_Aster (EDF Research and Development). The eigenvalue problem may be

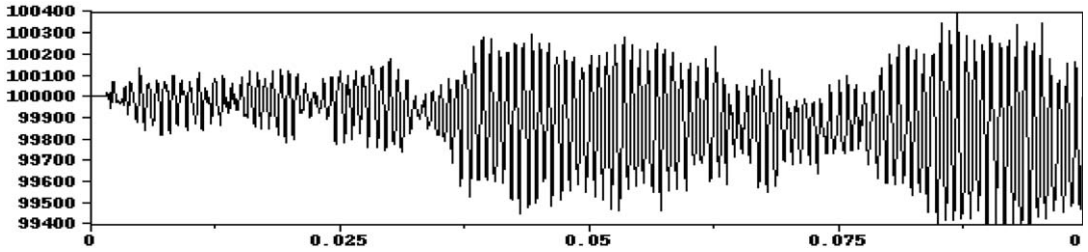

Fig. 7. Temporal evolution of the pressure at the top wall in front of the cavity.

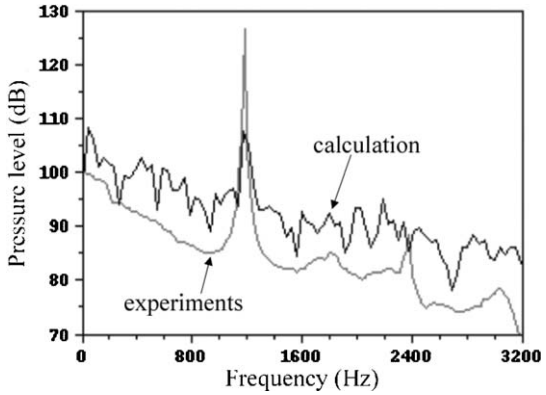

Fig. 8. Pressure spectra in the cavity in normalized form; $M_0 = 0.183$.

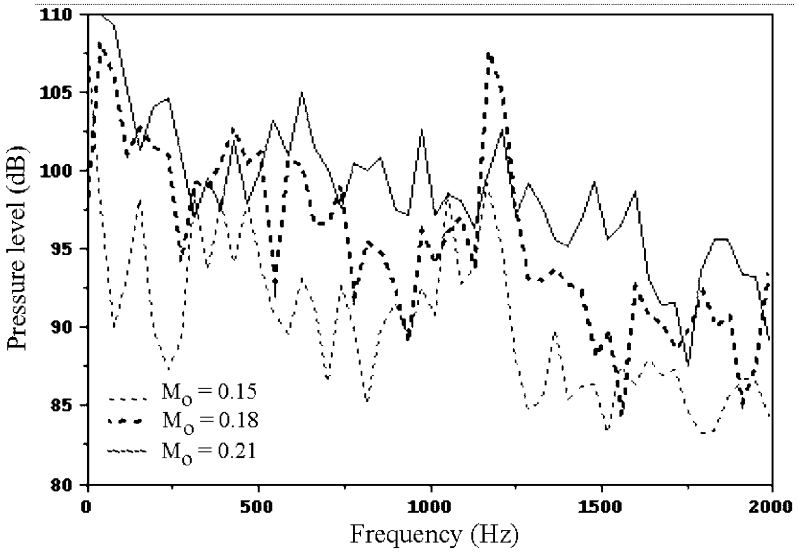

Fig. 9. Superposition of spectra for $M_0 = 0.15$, 0.183 and 0.21.

written as

$$\begin{pmatrix} K-\omega^2 M & 0 & -\omega^2\rho_f M_\Sigma \\ 0 & \dfrac{M_f}{\rho_f c_f^2} & -\omega^2\dfrac{M_{fl}}{c_f^2} \\ -\omega^2\rho_f M_\Sigma^{\mathrm{T}} & -\omega^2\dfrac{M_{fl}^{\mathrm{T}}}{c_f^2} & -\omega^2\rho_f H \end{pmatrix} \begin{pmatrix} u \\ p \\ \varphi \end{pmatrix} = \begin{pmatrix} 0 \\ 0 \\ 0 \end{pmatrix}, \tag{17}$$

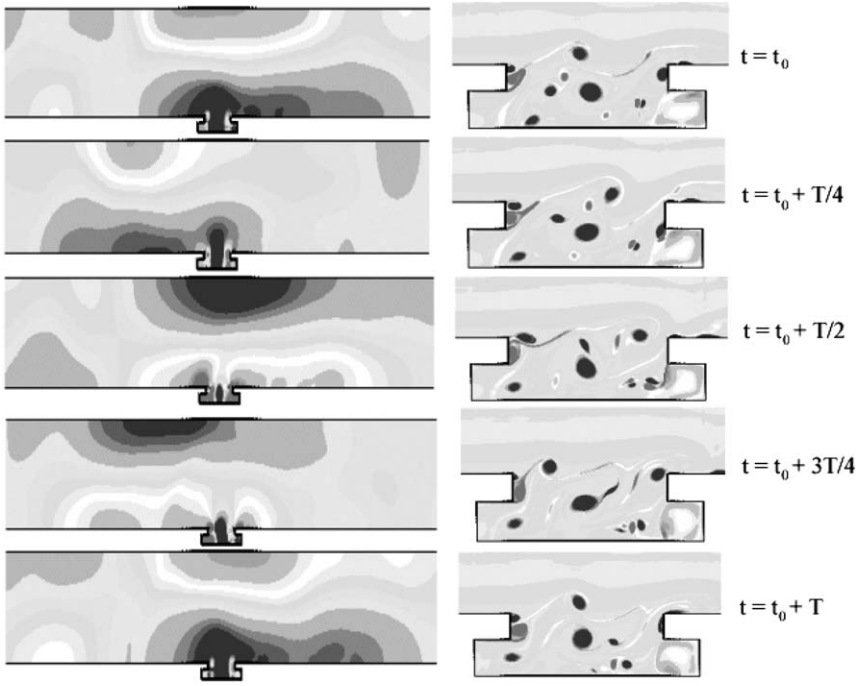

Fig. 10. Pressure and vorticity fields in the duct at $t_0, t_0 + T/4, t_0 + T/2, t_0 + 3T/4, t_0 + T$ during a high amplitude oscillation cycle ($t \cong 0.044$ s).

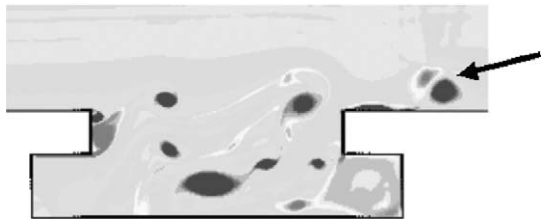

Fig. 11. Vorticity field in the duct during a low amplitude oscillation cycle ($t \cong 0.075$ s).

where K and M are the stiffness and mass matrices of the structure, M_Σ, M_f, M_{fl}, and H are given by the bilinear forms

$$M_\Sigma = \int_\Sigma u\varphi \, \mathrm{d}S, \tag{18}$$

$$M_f = \int_{\Omega_f} p^2 \, \mathrm{d}V, \tag{19}$$

$$M_{fl} = \int_{\Omega_f} p\varphi \, \mathrm{d}V, \tag{20}$$

$$H = \int_{\Omega_f} \left(\vec{\mathrm{grad}} \ \varphi \right)^2 \mathrm{d}V. \tag{21}$$

3.1.2. Analytical formulation of a cylindrical elastic shell filled with fluid

The fully coupled formulation used here is derived from De Jong (1994) who has used Flügge's cylindrical shell theory (Flügge, 1973). The problem may be written in cylindrical coordinates (x, r, θ). The local displacement variables

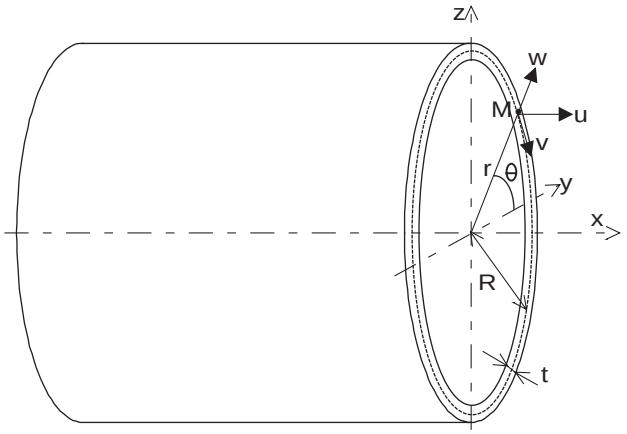

Fig. 12. Geometry of a pipe section.

u, v and w are associated to the cylindrical shell as shown in Fig. 12 and the fluid is characterized by its acoustical pressure p.

From the local equations of cylindrical shells, the displacements of the pipe may be written as a function of the axial wave number k_{nm} (De Jong, 1994; Fuller and Fahy, 1982) where $n(n \geqslant 0)$ is the order of circumferential modes and $m(m \geqslant 1)$ is the order of longitudinal modes:

$$u = \sum_{m=1}^{\infty} \sum_{n=0}^{\infty} U_{nm} \cos(n\theta) \mathrm{e}^{(\mathrm{j}\omega t + k_{nm} x + i\pi/2)}, \tag{22}$$

$$v = \sum_{m=1}^{\infty} \sum_{n=0}^{\infty} V_{nm} \sin(n\theta) \mathrm{e}^{(\mathrm{j}\omega t + k_{nm} x)},$$

$$w = \sum_{m=1}^{\infty} \sum_{n=0}^{\infty} W_{nm} \cos(n\theta) \mathrm{e}^{(\mathrm{j}\omega t + k_{nm} x)}.$$

The equation of Helmholtz for the fluid in cylindrical coordinates is

$$\frac{\partial^2 p}{\partial x^2} + \frac{\partial^2 p}{\partial r^2} + \frac{1}{r}\frac{\partial p}{\partial r} + \frac{1}{r^2}\left(\frac{\partial^2 p}{\partial \theta^2}\right) - \frac{1}{c_f^2}\frac{\partial^2 p}{\partial t^2} = 0. \tag{23}$$

From Eq. (23), the pressure p may be written as

$$p = \sum_{m=1}^{\infty} \sum_{n=0}^{\infty} P_{nm} \cos(n\theta) \mathrm{J}_n(\gamma_{mn} r) \mathrm{e}^{(\mathrm{j}\omega t + k_{nm} x)}, \tag{24}$$

where J_n is the Bessel's function J of the first kind of order n and γ_{mn} is the radial wave number. The wave numbers are related by the equation

$$k_f^2 = k_{nm}^2 - \gamma_{nm}^2 \quad \text{with} \quad k_f = \mathrm{j}\omega/c_f. \tag{25}$$

The boundary condition between the fluid and the pipe may be written as (De Jong, 1994; Fuller and Fahy, 1982)

$$\left.\frac{\partial w}{\partial t}\right|_{r=R_i} = -\frac{1}{\mathrm{j}\rho_f \omega}\frac{\partial p}{\partial r}, \tag{26}$$

then

$$P_{nm} = \frac{\omega^2 \rho_f}{\gamma_{nm} \mathrm{J'}_n(\gamma_{nm} R_i)} W_{nm}, \tag{27}$$

where R_i is the inside pipe radius ($R_i = R - t/2$). The fluid–structure problem may be written for a given (n, m) as

$$\begin{pmatrix} L_{11} & L_{12} & L_{13} \\ L_{21} & L_{22} & L_{23} \\ L_{31} & L_{32} & L_{33} \end{pmatrix} \begin{pmatrix} U_{nm} \\ V_{nm} \\ W_{nm} \end{pmatrix} = \begin{pmatrix} 0 \\ 0 \\ 0 \end{pmatrix}, \tag{28}$$

where the matrix L may be expressed using Flügge's shell theory coupled with the fluid (De Jong, 1994). Fuller and Fahy (1982) have used Donnell's shell theory to express the matrix L, which is known to be less complete (Blevins, 1979):

$$\begin{aligned} L_{11} &= \Omega^2 + \kappa_{nm}^2 - \frac{1-\nu}{2} n^2(1+\beta^2), \quad L_{22} = \Omega^2 + \frac{1-\nu}{2} \kappa_{nm}^2(1+3\beta^2) - n^2, \\ L_{33} &= 1 - \Omega^2 - FL + \beta^2[1 - 2n^2 + (n^2 - \kappa_{nm}^2)^2], \quad L_{12} = L_{21} = j \frac{1+\nu}{2} \kappa_{nm} n, \\ L_{13} &= L_{31} = \kappa_{nm}\left[\nu - \beta^2\left(\kappa_{nm}^2 + \frac{1-\nu}{2} n^2\right)\right], \quad L_{23} = L_{32} = \mathrm{j}n\left(1 - \frac{3-\nu}{2} \beta^2 \kappa_{nm}^2\right), \end{aligned} \tag{29}$$

where

$$FL = \Omega^2 \frac{\rho_f R_i^2}{\rho_s t R} \frac{\mathrm{J}_n(\gamma_{nm} R_i)}{\gamma_{nm}^i R_i \mathrm{J}'_n(\gamma_{nm} R_i)} \quad \text{and} \quad \beta^2 = \frac{t^2}{12R^2} \tag{30}$$

and Ω and κ_{nm} are, respectively, the nondimensional frequency and the nondimensional longitudinal wave number:

$$\Omega = \frac{f}{f_{\text{ring}}} \quad \text{and} \quad f_{\text{ring}} = \frac{1}{2\pi R}\sqrt{\frac{E}{\rho_s(1-\nu^2)}} \tag{31}$$

and

$$\kappa_{nm} = k_{nm} R, \tag{32}$$

where f_{ring} is the ring frequency. The dispersion equation of the problem is then derived from the determinant of the matrix L:

$$\det(L) = 0. \tag{33}$$

Eq. (33) may be solved using the series expansion for the Bessel functions, which is well detailed for instance by De Jong (1994) or Pavic (1990). A specific program has been developed using Matlab software to calculate dispersion curves (longitudinal wave numbers as a function of the frequency).

3.2. Application

3.2.1. Description of the piping system

The main objective of the study is to explicate the fluid–structure phenomenon, which occurs in the steam line and allows the energy transfer from the fluid to the main pipe. An experimental modal analysis has been realized on the main pipe outside the reactor building, in the lower part. These tests show that the pipe deformations combine flexion and ovalization around 460 Hz. No accurate test could be done using pressure sensors as the line is safety-related and data on the pressure field in the fluid are not available. Nevertheless, two scenarios may be possible: there may be plane waves, which are well known in low frequencies (De Jong, 1994; Seligmann et al., 1998) or transverse acoustical waves, which is coherent with the flow-acoustical analysis of the gate valve.

This steam line is limited by a steam generator and a clamped end point, which is outside the reactor building (Fig. 13). The steam line crosses the reactor building through penetration. The pipe is made of stainless steel and its couple of data (outer diameter; thickness) is varying from the steam generator (762; 35 mm) to the clamped end (786; 48 mm). The radius of curvature of the elbows is large. The gate valve nominal diameter is less than the main pipe diameter. The elbows are not well represented in Fig. 13, which is not the case in Figs. 14 and 15. Close to the operating pressure, the steam density and its sound celerity are approximately of 40 kg/m^3 and 500 m/s, respectively. The Mach number is quite low inside the pipe, which supposes that flow effects may be neglected for these vibroacoustical analysis.

3.2.2. FEM analysis

To analyse fluid–structure coupling effects in the frequency range 400–500 Hz, a simplified model of the steam line including only the main pipe with its clamped end boundary conditions has been built up. The penetration of the reactor building is modelled using a static stiffness. In this medium frequency range, boundary conditions effects,

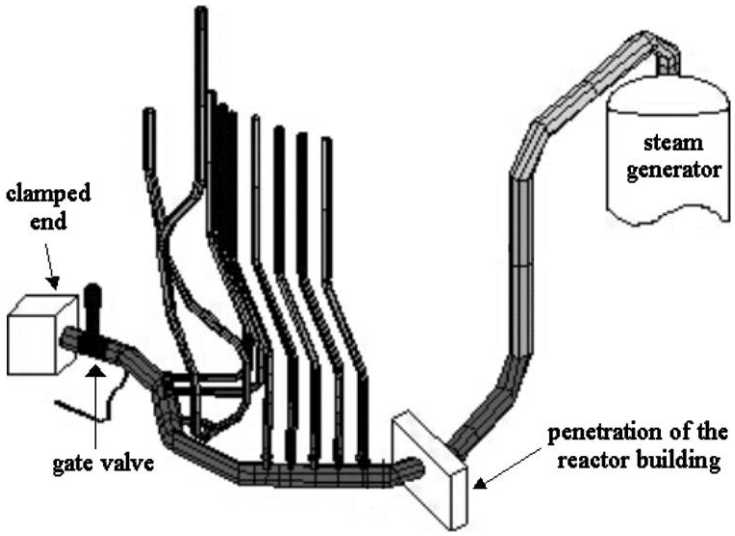

Fig. 13. Simplified representation of the line.

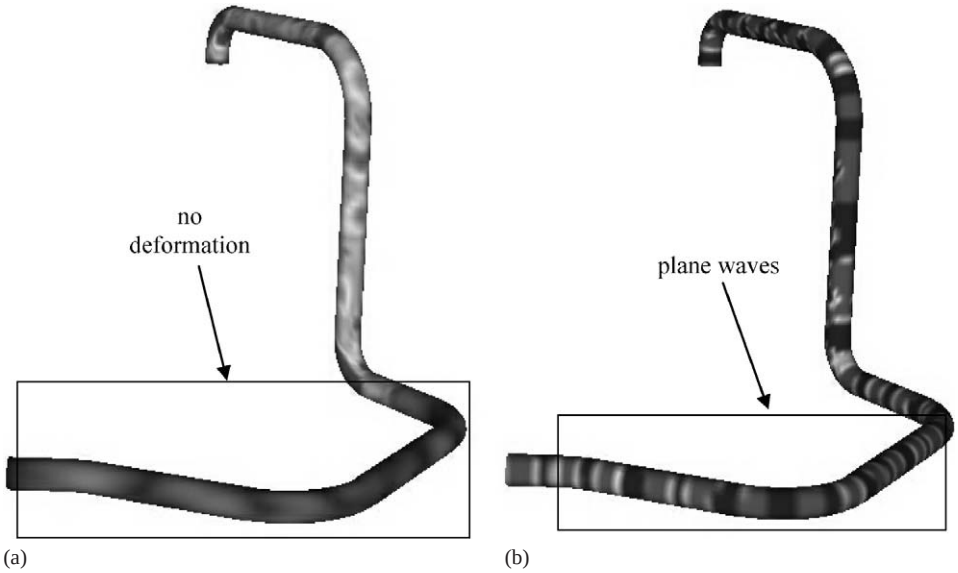

Fig. 14. Plane waves acoustical mode. (a) Deformation of the pipe and (b) pressure field in the fluid.

influence of the models of supports, influence of connected pipes, etc. are shown to be weak, which is not the case in low frequencies. Different levels of model (representations of the valve, of some supports, etc.) have been tested and did not show significant differences in the results. And, the objective of the analysis is only qualitative, an accurate and complete model of the steam line is not necessary here.

The FE model of the pipe uses discrete shear quadrilateral (DST) shell elements of Batoz and Dhatt (1990) for the pipe and (p, φ) 3D-acoustics FE for the fluid (Morand and Ohayon, 1995). The coupled model is then constituted of approximately 65 000 degrees of freedom. The modes are calculated in the frequency range 400–500 Hz. In this frequency range, the modal density, which is of approximately 50 modes, is quite important and only the most participating modes representing the major part of the physical mass are selected (here, 11 modes).

Most of the modes calculated are shown to exhibit transverse acoustical pressure fields. Nevertheless, we observe once a mode with plane waves (Fig. 14(b)). But, for this mode, there is no deformation of the pipe between the clamped

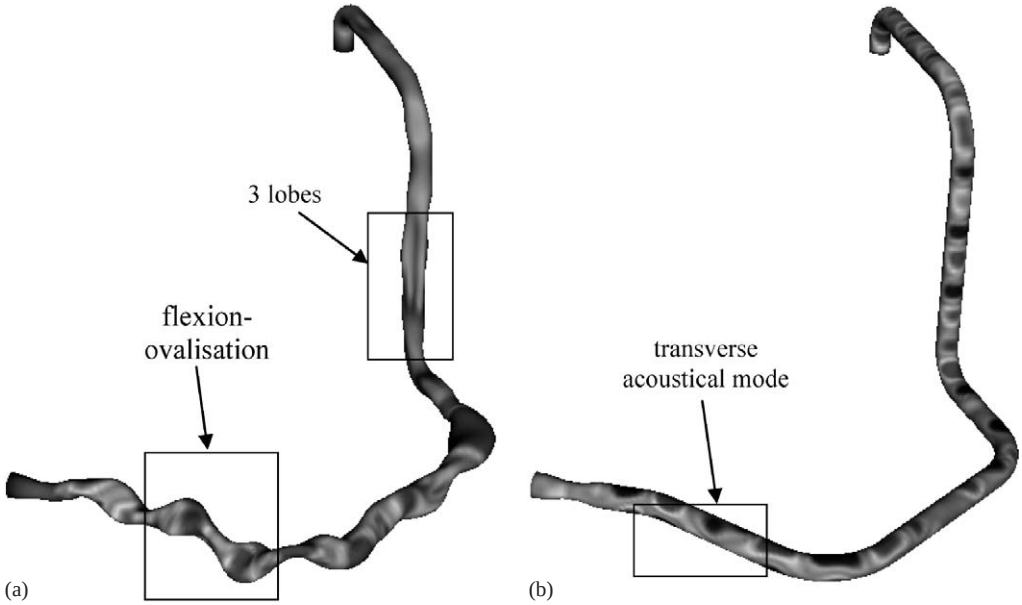

Fig. 15. Transverse acoustical waves coupled with flexural-ovalization waves of the pipe. (a) Deformation of the pipe and (b) pressure field in the fluid.

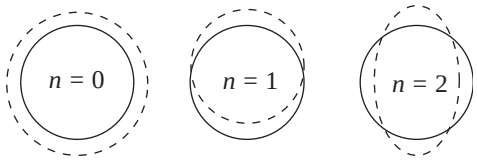

Fig. 16. Shapes of circumferential modes of order n.

end and the reactor building (Fig. 14(a)). Finally, the coupling effects between the pipe and acoustical plane waves are shown to be weak in the frequency range analysed.

For the frequency of 460 Hz, which is close to the excitation frequency of the gate valve, one mode exhibits transverse acoustical waves coupled with flexion-ovalization deformations in the lower part of the steam line (Fig. 15). Other modes also have the same behaviour but the mode presented here is the most illustrating. The dynamic behaviour combining flexion-ovalization deformations is close to that observed with the experiments. In Fig. 15, the longitudinal wavelengths of the pressure field and of the deformation of the pipe are quite similar. Finally, the transverse acoustical waves scenario is validated using a simplified FE model of the steam line.

3.2.3. *Dispersion analysis*

The fully coupled formulation of Section 3.1.2 is available for one couple of data (outer diameter, thickness). As the outer diameter and the thickness are not constant along the pipe, the dispersion analysis may be conducted for each part of the steam line. Nevertheless, we are presenting here the results with the couple of data in the lower part (diameter, thickness), which is sufficient to explain the fluid–structure coupling effects acting in the piping system. One notes that the present dispersion analysis is local in opposition to the FEM analysis which is global and includes the whole pipe.

The dispersion curves are function of order n of the circumferential modes of Fourier (in cylindrical coordinates: $\cos(n\theta)$ as in Eq. (22)):

(i) $n = 0$ corresponds to an extension and torsion (which are not studied here) of the pipe and to plane waves in the fluid (Fig. 16),
(ii) $n = 1$ corresponds to flexural vibration of the pipe and to transverse acoustical modes,
(iii) $n = 2$ corresponds to ovalization of the pipe and to acoustical modes with 2 lobes,
(iv) finally n corresponds to modes with n lobes.

As the formulation used here is fully coupled, dispersion curves inherent to the fluid or to the pipe cannot be distinguished. Nevertheless, the fully coupled dispersion diagram of Fig. 17 may be compared to the uncoupled one of Fig. 18, where the fluid and solid dispersion curves are different. When a solid dispersion curve crosses a fluid one of the same order n, the fluid–structure coupling may be strong. In that case, the time scale (i.e. the frequency) and the spatial

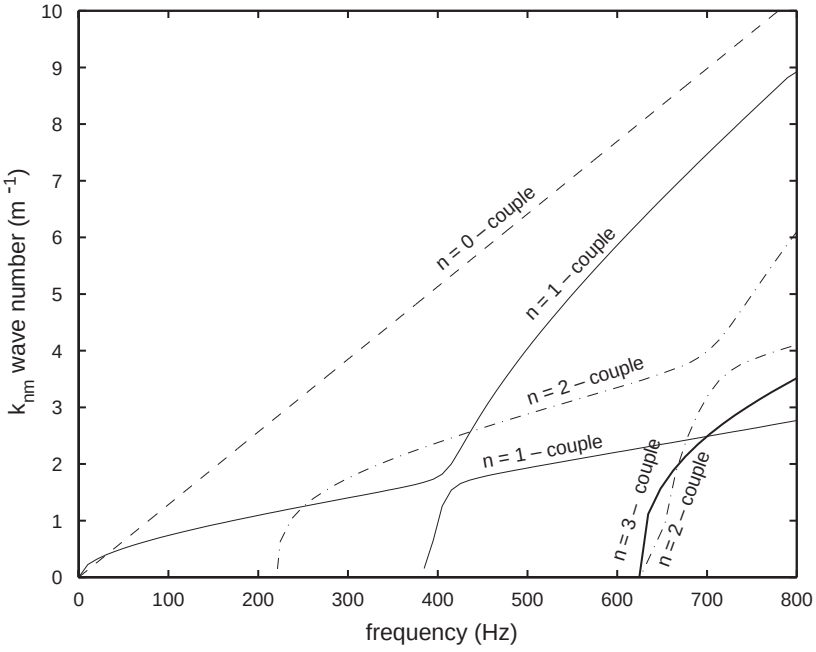

Fig. 17. Fully coupled dispersion diagram.

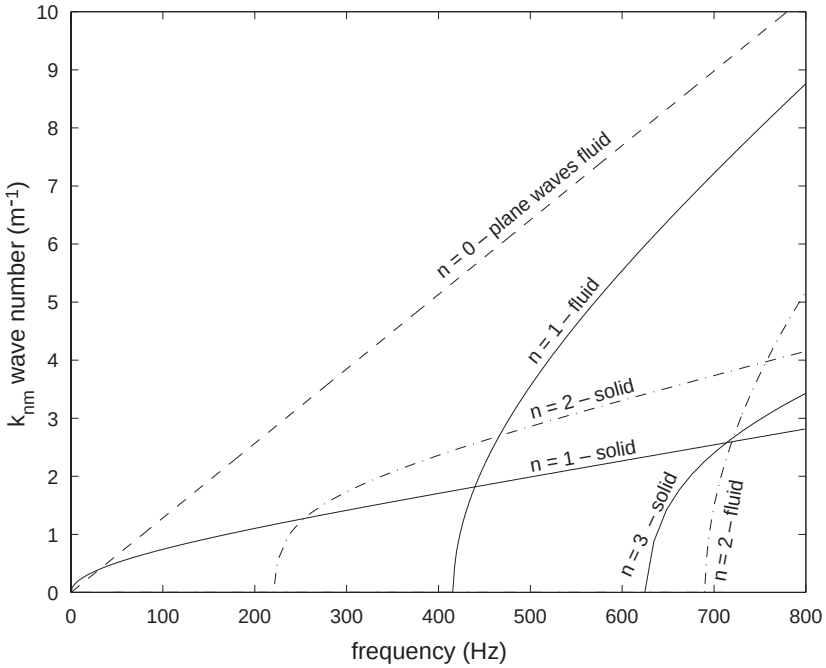

Fig. 18. Uncoupled dispersion diagram.

scale (i.e. the wave number) of the fluid and of the solid are equivalent. Finally, the dispersion diagram of Fig. 17 shows that there is a strong coupling between the modes of order $n = 1$ around 420 Hz and $n = 2$ around 700 Hz.The dispersion analysis leads to the following conclusions in the frequency range 400–500 Hz:

1. there may be strong fluid–structure coupling between flexural modes and transverse acoustical modes,
2. the flexural or ovalization modes of the pipe cannot couple with the plane waves in the fluid because the waves numbers are not equivalent, which is not the case in low frequency for flexion,
3. the flexural modes may be coupled with the ovalization ones because the wave numbers are equivalent. One notes that a straight pipe cannot have combined flexion and ovalization deformations. In that case the modes of Fourier $\cos(n\theta)$ are 'pure'. To be coupled the flexion of the pipe must excite its ovalization and conversely, which is the case in elbows.

The qualitative conclusions obtained here are equivalent to that of the FEM analysis and of the experiments.

3.3. Discussion

The global fully coupled method (i.e. FEM) as well as the local one (i.e. dispersion analysis) lead to the same qualitative conclusion. The modal analysis realized on a simplified model of the steam line shows that the results are quite independent of the boundary conditions, of the presence of supports, etc. Finally, the vibrations of the pipe in the medium frequency range 400–500 Hz exhibit a local behaviour. An indicator of this local behaviour may be the longitudinal wavelengths which are short compared to the total pipe length (Fig. 14). This observation validates the use of dispersion diagrams based on cylindrical shells to analyse fluid–structure coupling in pipes in middle frequency.

The dispersion analysis is performed here on one pipe section (outer diameter 686 mm; thickness 48 mm), which is representative of the steam line from the reactor building to the clamped end (lower part). Inside the reactor building, the thickness of the pipe is less important. In that case, the dispersion diagram shows that the pipe may exhibit modes of Fourier with 3 lobes which is validated by the FEM calculations in Fig. 14. The cut-on frequency of modes with 3 lobes is of 620 Hz outside the reactor building (Fig. 14) and of 450 Hz inside. These frequencies are read on dispersion diagrams but may also be calculated using the following equation of De Jong (1994):

$$f_n^{\text{cut-on}} = f_{\text{ring}} \frac{\beta n(n^2-1)}{\sqrt{1+n^2+2n\dfrac{\rho_f A_f}{\rho_s A_s}}}, \tag{34}$$

where β is given in Eq. (30), A_f and A_s are the areas of fluid and solid and n the order of the mode of Fourier. Finally, in a first approach, the possible modes of deformation of a pipe may be estimated using Eq. (34).

The use of dispersion diagrams alone may be sufficient to analyse fluid–structure coupling in pipes in middle frequency:

1. the possible modes of Fourier for a given frequency may be calculated using Eq. (34) or dispersion diagrams. One notes that when the wave number is zero, the corresponding wavelength is infinite. Then, these cut-on frequencies correspond to pipes of infinite lengths.
2. the frequency ranges of strong coupling may be easily defined. Strong coupling occurs when the time scale (i.e. the frequency) and the spatial scale (i.e. the wave number) of the solid and the fluid are equivalent.

Nevertheless, this approach is only qualitative. The use of FEM or other numerical methods is essential to evaluate levels of vibration.

4. Conclusion

In order to study a cavity noise phenomenon occurring in an industrial valve, experiments and computations on 2-D and 3-D configurations are planned. Results from 2-D computations are presented here. The modelling approach is based on Euler equations and so physical viscosity is not taken into account. Due to this limitation, only qualitative results are obtained when the pure Euler computation is carried out. But, when a viscous correction, based on experimental data, is applied on the boundary layer upstream the cavity, all essential results are retrieved: frequencies of oscillation and cavity/duct coupling. Calculations are achieved to show the evolution of the phenomena with respect to the nominal velocity and especially to display when the cavity/duct coupling starts and when it stops.

Two fully coupled methods based on FEM and dispersion diagrams are tested to evaluate fluid–structure coupling effects on a PWR steam line. Both methods exhibit the way of energy transfer, which is transverse acoustical modes coupled with combined flexion-ovalization deformations of the pipe. The link between the analysis of the fluid/acoustic excitation of Section 2 and of the fluid/structure coupling of Section 3 is the excitation of the transverse acoustical mode of the duct. This industrial problem is a good illustration of 3 different coupling phenomena, which may occur in flexible structure under fluid flow:

1. a flow-acoustic coupling in a shallow cavity appears inside the gate valve at the nominal flow velocity,
2. this aeroacoustical phenomenon of Rossiter is then coupled with the transverse acoustical mode of the pipe,
3. which is finally coupled with combined flexion-ovalization deformations of the pipe.

In a second step, it may be interesting to get a quantitative approach using FEM to evaluate levels of vibration. In that case, a complete model of pipe is essential to evaluate zones of maximum stress and displacement. It may also be fundamental to proceed with the aeroacoustical analysis on 3D configurations to find an industrial solution, which suppresses or reduces the cavity noise source in the gate valve.

Acknowledgements

The authors wish to thank Bruce Smith from Atomic Energy of Canada Limited for useful information in finding solutions to suppress aeroacoustical coupling effects in the gate valve.

References

Amandolèse, X., Hémon, P., Regardin, C., 2002. Study of the acoustic oscillations by flows over cavities. Part 1. Internal flows. In: Proceedings of the Fifth International Symposium on Fluid-Structure Interactions, IMECE'02, New Orleans.

Axisa, F., 2001. Modélisation des systèmes Mécaniques, Tome 3: Interactions Fluide Structure. Hermès, Paris.

Batoz, J.-L., Dhatt, G., 1990. . Modélisation des structures par éléments-finis, Poutres et plaques, Vol. 2. Hermès, Paris.

Blevins, R.D., 1979. Formulas for Natural Frequency and Mode Shape. Van Nostrand Reinhold Company, NY.

Blevins, R.D., 2001. Flow-Induced Vibration 2nd Edition. Krieger Publishing Company, Malabar, FL.

De Jong, C.A.F., 1994. Analysis of pulsations and vibrations in fluid pipe systems. Ph.D. Thesis, Technische Universiteit Eindhoven, The Netherlands.

Dequand, S., Hulshoff, S., Van Kuijk, H., Willems, J., Hirschberg, A., 2003. Helmholtz-like resonator self-sustained oscillations, Part 2: detailed flow measurements and numerical simulations. AIAA Journal 41 (3), 416–423.

Devos, J.P., Lambert, C., 2001. Analyse expérimentale 2D du comportement aéroacoustique d'une vanne vapeur. Clamart (Fr.): EDF, Technical Note HT-63/01/019/B.

Flügge, W., 1973. Stresses in Shells. 2nd Edition. Springer, Berlin, Germany.

Fuller, C.R., Fahy, F., 1982. Characteristics of wave propagation and energy distributions in cylindrical elastic shells filled with fluid. Journal of Sound and Vibration 81 (4), 501–518.

Gibert, R.-J., 1988. Vibrations des structures, Interaction avec les Fluides, Sources d'Excitation Aléatoires. Eyrolles, Paris.

Gloerfelt, X., 2001. Calcul aéroacoustique direct du bruit rayonné par un écoulement affleurant une cavité et analyse de méthodes intégrales. Ph.D. Thesis, Ecole Centrale de Lyon, Lyon, France.

Gloerfelt, X., Bailly, C., Juvé, D., 2003. Direct computation of the noise radiated by a subsonic cavity flow and application of integral methods. Journal of Sound and Vibration 266 (1), 119–146.

Harten, A., 1983. High resolution schemes for hyperbolic conservation laws. Journal of Computational Physics 49, 357–393.

Keller, J.J., Escudier, M.P., 1983. Flow-excited resonances in covered cavities. Journal of Sound and Vibration 86, 199–226.

Lafon, P., Devos, J.P., 1993. Numerical prediction of instabilities in transonic internal flows using an Euler TVD code. In: Proceedings of the 31st Aerospace Sciences Meeting, Reno, Nevada.

Lafon, P., Lambert, C., Devos, J.-P., Caillaud, S., 2002. Aeroacoustical coupling and its structural effects on a PWR steam line. Part 1. Numerical investigations of flow acoustic coupling in a subsonic flow past a shallow cavity. In: Proceedings of the Fifth International Symposium on Fluid–Structure Interactions, IMECE'02, New Orleans.

Morand, H.J.-P., Ohayon, R., 1995. Fluid Structure Interaction. Wiley, NY.

Ohayon, R., Valid, R., 1981. True symmetric formulations of free vibrations of fluid-structure interaction. Applications and extension. In: Conference Proceedings, Numerical Methods for Coupled Problems. Pineridge Press, Swansea, UK, pp. 335–355.

Pavic, G., 1990. Vibration energy flow in elastic circular cylindrical shells. Journal of Sound and Vibration 142 (2), 293–310.

Pavic, G., 1992. Vibroacoustical energy flow in elastic circular cylindrical shells. Journal of Sound and Vibration 143 (3), 411–429.

Poinsot, T.J., Lele, S.K., 1992. Boundary conditions for direct simulations of compressible viscous flows. Journal of Computational Physics 101, 104–129.

Roe, P.L., 1980. Approximate Riemann solvers, parameters vectors, and difference schemes. Journal of Computational Physics 43, 357–372.

Rossiter, J.E., 1964. Wind-tunnel experiments on the flow over rectangular cavities at subsonic and transonic speeds. Aeronautical Research Council Reports and Memoranda. Technical Report 3438.

Rockwell, D., Naudascher, E., 1978. Review—self-sustained oscillations of flow past cavities. Journal of Fluids Engineering 100, 152–165.

Rockwell, D., Lin, J.-C, Oshkai, P., Reiss, M., Pollack, M., 2003. Shallow cavity flow tone experiments: onset of lock-on states. Journal of Fluids and Structures 17 (3), 381–414.

Sarohia, V., 1977. Experimental oscillations in flows over shallow cavities. AIAA Journal 15 (7), 984–991.

Seligmann, D., Fournier, I., Guillou, J., 1998. Flow induced vibration in piping systems using CIRCUS software. In: Proceedings of the Pressure Vessels and Piping Conference, Vol. 366. ASME PVP, Boston, pp. 227–233.

Smith, B.A.W., Luloff, B.V., 1999. The effect of seat geometry on gate valve noise. In: Proceedings of the Pressure Vessels and Piping Conference, Vol. 389. ASME PVP, Boston, pp. 299–306.

Yee, H.C., Klopfer, G.H., Montagne, J.L., 1990. High resolution shock-capturing schemes for inviscid and viscous hypersonic flows. Journal of Computational Physics 88, 31–61.